

XMM-Newton observations of the temperature structure of the central gas in cooling clusters

Jelle S. Kaastra,¹ Takayuki Tamura,^{1,2} John R. Peterson,³ Johan A.M. Bleeker,¹ Carlo Ferrigno,^{1,4} Steve M. Kahn,^{3,5} Frits B.S. Paerels,³ Rocco Piffaretti,^{6,7} Graziella Branduardi-Raymont,⁸ and Hans Böhringer⁹

¹ *SRON National Institute for Space Research, Sorbonnelaan 2, 3584 CA Utrecht, The Netherlands*

² *Institute of Space and Astronautical Science (ISAS), 3-1-1 Yoshinodai, Sagami-hara, Kanagawa 229-8510, Japan*

³ *Columbia Astrophysics Laboratory, Columbia University, 550 West 120th Street, New York, NY 10027, USA*

⁴ *Istituto di Astrofisica Spaziale e Fisica Cosmica, Sezione di Palermo, Via Ugo La Malfa 153 90146 Palermo, Italy*

⁵ *Kavli Institute for Particle Astrophysics and Cosmology, Stanford University, Stanford, CA 94305, USA*

⁶ *Institute of Theoretical Physics, University of Zürich, Winterthurerstrasse, 190, CH-8057 Zürich, Switzerland*

⁷ *Paul Scherrer Institute, Laboratory for Astrophysics, CH-5232 Villigen, Switzerland*

⁸ *Mullard Space Science Laboratory, University College London, Holmbury St. Mary, Dorking, Surrey, RH5 6NT, UK*

⁹ *Max-Planck-Institut für extraterrestrische Physik, Giessenbachstrasse, 85748 Garching, Germany*

We present spatially resolved X-ray spectra taken with the EPIC cameras of *XMM-Newton* of a sample of 17 cooling clusters and three non-cooling clusters for comparison. The deprojected spectra are analyzed with a multi-temperature model, independent of any a priori assumptions about the physics behind the cooling and heating mechanisms. All cooling clusters show a central decrement of the average temperature, most of them of a factor of ~ 2 . Three clusters only show a weak temperature decrement, while two others have a very strong temperature decrement. At each radius within the cooling region the gas is not isothermal. The differential emission measure distribution shows a strong peak near the maximum (ambient) temperature, with a steep decline towards lower temperatures, approximately proportional to T^3 , or alternatively a cut-off at about a quarter to half of the maximum temperature. In general, we find a poor correlation between radio flux of the central galaxy and the temperature decrement of the cooling flow. This is interpreted as evidence that except for a few cases (like the Hydra A cluster) heating by a central AGN is not the most common cause of weak cooling flows. We investigate the role of heat conduction by electrons and find that the theoretically predicted conductivity rates are not high enough to balance radiation losses. The differential emission measure distribution has remarkable similarities with the predictions from coronal magnetic loop models. Also the physical processes involved (radiative cooling, thermal conduction along the loops, gravity) are similar for clusters loops and coronal loops. If coronal loop models apply to clusters, we find that a few hundred loops per scale height should be present. The typical loop sizes deduced from the observed emission measure distribution are consistent with the characteristic magnetic field sizes deduced from Faraday rotation measurements.

1. Introduction

In the central part of clusters of galaxies the gas density is high. There the radiative cooling time is shorter than the age of the cluster. The temperature decreases due to radiative cooling. The corresponding pressure decrease then causes a net inflow towards the center of the cluster, the so-called cooling flow. In the isobaric cooling flow model gas cools in pressure equilibrium with its surroundings. The amount of gas at each temperature is controlled by how fast it can cool, i.e. the radiative cooling rate through—mainly—X-ray radiation.

The first high-resolution X-ray spectra of clusters of galaxies taken with the Reflection Grating Spectrometers

(RGS) of *XMM-Newton* showed indeed the presence of cooler gas in the cores of several clusters. However, the amount of cool gas at lower temperatures was much smaller than predicted by the isobaric cooling flow model (Sérsic 159–3, Kaastra et al. 2001; A 1835, Peterson et al. 2001; A 1795, Tamura et al. 2001a). The second paper also contains a list of possible explanations for this phenomenon.

This discovery has triggered a series of papers offering a broad range of explanations for the apparent failure of the isobaric cooling flow model. Several of these are presented at this conference.

The lack of relatively cool gas has been confirmed by the RGS spectra of other clusters, like A 496 (Tamura et

al. 2001b) and Virgo (Sakelliou et al. 2002)). The lack of this cool gas is deduced from both RGS and EPIC data. These EPIC data have also been reported in the RGS papers mentioned above. In addition, Molendi & Pizzolato (2001) found evidence for an apparent low temperature cut-off in the cooling gas at about 1–2 keV in the EPIC spectra of A 1835, A 1795 and Virgo, while Matshushita et al. (2002) report that the EPIC data of Virgo show that the cool gas has a single temperature at each radius.

Also *Chandra* observations have confirmed the lack of cool gas in clusters. In Hydra A (David et al. 2001) the gas has essentially a single temperature at each radius between 30–200 kpc, with a steadily outwards temperature increase. Only in the innermost 30 kpc there is evidence for multi-phase gas, however with a ten times smaller mass deposition rate as derived from the morphologically derived mass accretion rate at 30 kpc.

The superb energy resolution of the RGS allowed a detailed investigation of the temperature structure of the core. Although the RGS has spatial resolution in the cross dispersion direction of the gratings, for most of the available data the statistics are not good enough to map the cool gas in the cross dispersion direction. In order to be able to distinguish between the various theoretical models that have been proposed, it is important to measure the temperature structure for each radius. As shown above, for some clusters a single-phase cooling gas distribution at each radius has been measured (Hydra A, David et al. 2001; Virgo, Matshushita et al. 2002; A 2029, Lewis et al. 2002).

Here we report on a study of a large sample of clusters and use the spatially resolved *XMM-Newton*/EPIC spectra to investigate the temperature structure at each radius. These measurements allow us to distinguish between isothermal, isobaric cooling or cut-off cooling flow models. More details about this analysis are given by Kaastra et al. (2003).

2. Analysis

2.1. Cluster Sample

The data analysis is described extensively by Kaastra et al. (2003). Here we summarize the results. Our sample of clusters (Table 1) consists of 17 cooling clusters and for comparison 3 non-cooling clusters (A 3266, Coma and A 754). Temperatures range between 1–15 keV, and most clusters have intermediate redshift (0.02–0.07). Our sample comprises the clusters used by Peterson et al. (2003) in their analysis of the RGS spectra. In our analysis, we assume spherical symmetry and we use deprojected spectra. Data obtained by the MOS and pn detectors were fitted simultaneously.

As a first step, we fitted single temperature models to our spectra. Later, we consider more complex spectral models.

2.2. Consistency with *Chandra*

In order to investigate how much our results depend upon the specific properties of the EPIC instruments, we checked the consistency of our results with *Chandra*.

TABLE 1. BASIC CLUSTER PARAMETERS

Cluster	z^a	scale ^b	kT^c	F_X^d	N_H^e
NGC 533	0.0175	30	1.3	6	3.00
Virgo	0.0027	4.7	2.4	821	1.80
A 262	0.0155	26	2.4	49	8.94
A 1837	0.0707	109	2.4	7	4.38
Sérsic 159–3	0.0572	90	2.5	24	1.79
MKW 9	0.0402	65	2.7	2.3	4.18
2A 0335+096	0.0344	57	3.0	81	28.71
MKW 3s	0.0455	73	3.0	30	2.89
A 2052	0.0356	58	3.1	47	2.91
A 4059	0.0466	75	3.5	31	1.06
Hydra A (A 780)	0.0550	87	3.8	48	4.80
A 496	0.0322	53	3.9	75	6.44
A 3112	0.0756	116	4.1	36	2.61
A 1795	0.0639	100	5.3	68	1.01
A 399	0.0706	109	5.8	29	10.90
A 3266	0.0614	96	6.2	49	1.60
Perseus (A 426)	0.0179	30	6.3	926	14.90
Coma (A 1656)	0.0240	40	8.1	319	0.89
A 754	0.0561	89	9.1	64	5.67
A 1835	0.2541	298	14.8	15	2.32

^a Redshift, to be used for the distance estimate.

^b Angular scale, in kpc/arcmin.

^c Temperature, in keV.

^d Unabsorbed 0.1–2.4 keV X-ray flux, in 10^{-15} W m⁻².

^e Galactic column density, in 10^{24} m⁻².

To do this, we compared deprojected, single temperature fits. Fig. 1 shows the comparison of our single temperature profile with the *Chandra* data as published by Blanton et al. (2003). At radii smaller than 30 arcsec, *Chandra* clearly benefits from its superior spatial resolution. However, the average temperature as found in the innermost annulus of the *XMM-Newton* data is fully consistent with the average temperature as derived from the *Chandra* data. At intermediate radii (0.5–6 arcmin) the cluster shows less spatial structure, and the profiles derived from both satellites agree well. Note that due to the larger effective area of *XMM-Newton*, the statistical error bars on the *XMM-Newton* data are significantly smaller than the error bars on the *Chandra* data, despite the shorter exposure time for the *XMM-Newton* observation. At large radii, the temperature shows a steep decline, and this is only visible in the *XMM-Newton* data since the field of view of *Chandra* is smaller.

2.3. Single Temperature Fits

The temperature profiles that we derive from our single temperature fits for the inner, cooling parts of the clusters that we studied are consistent with the formula proposed by Allen et al. (2001):

$$T(r) = T_c + (T_h - T_c) \frac{r^2}{r_c^2 + r^2}. \quad (1)$$

In this equation, r_c is a scale parameter for which we

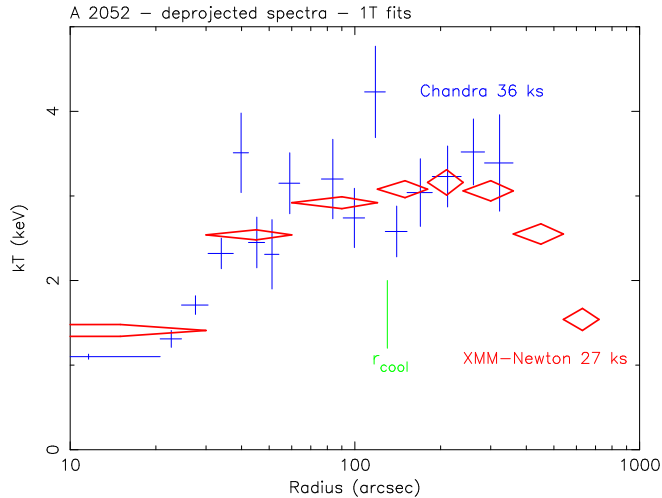


FIG. 1.— Comparison of the deprojected single temperature profiles of A 2052. *XMM-Newton* EPIC data: Kaastra et al. (2003); *Chandra* ACIS data: Blanton et al. (2003).

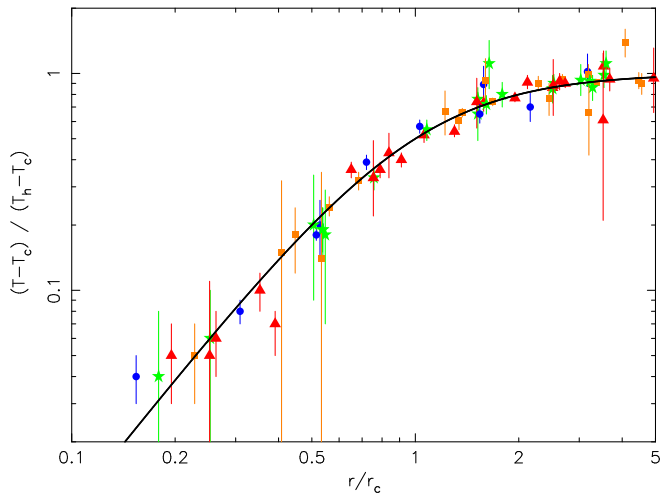


FIG. 2.— Scaled temperature profiles versus scaled radius. Temperatures have been normalized as indicated using the temperature T_h of the hot gas outside the cooling region as well as the central temperature T_c . Red triangles: clusters cooler than 3 keV; orange squares: clusters with temperatures from 3–4 keV; green stars: clusters with temperatures from 4–6 keV; blue circles: clusters with temperatures above 6 keV. The non-cooling clusters Coma, A754 and A 3266 have been omitted from the plot. The solid line is the scaling curve Eq. (1).

find best-fit values between 20–100 kpc. The parameter T_c corresponds to the temperature at the center of the cluster ($r = 0$), while T_h is the asymptotic temperature at large radii (since we consider in this paper the central cooling region, we ignore here the temperature drop at large radii that we find in some of our clusters; that drop always occurs well outside the cooling region). We find that the relative temperature decrement at the core, given by the ratio $(T_h - T_c)/T_h$ has values between 0.15–0.70 for our cluster sample. We show the scaled temperature profiles in Fig. 2.

There exist some scaling laws between the parameters of our fit to Eq. (1). For instance, there is a correlation between characteristic radius r_c and asymptotic temper-

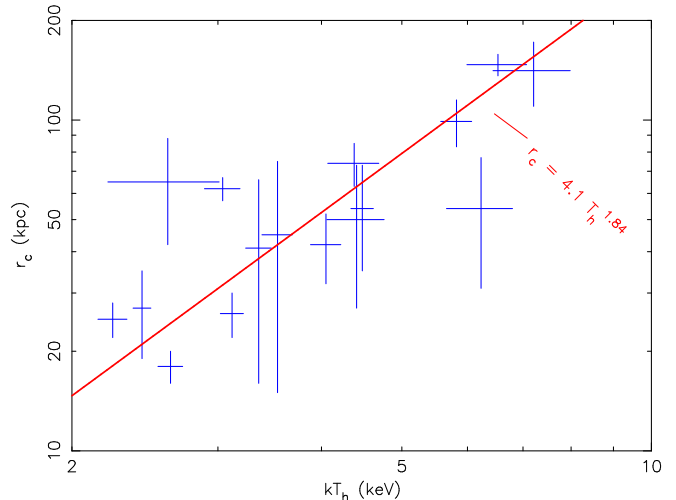


FIG. 3.— Characteristic radius r_c versus asymptotic temperature T_h at large radii. The solid line shows the best-fit power law through these data.

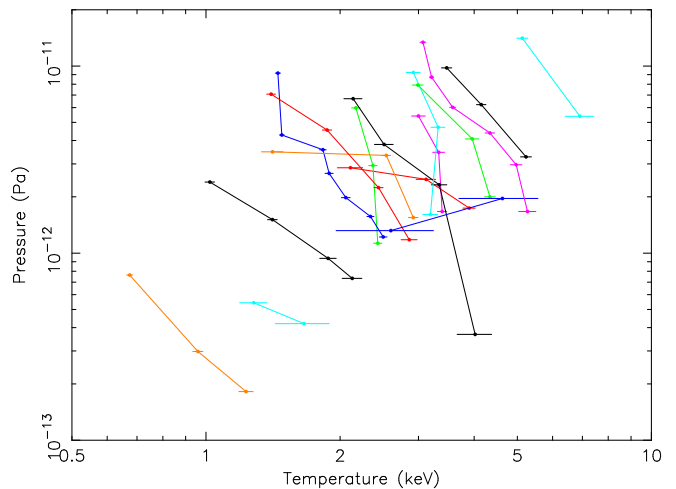


FIG. 4.— Pressure versus temperature for 16 clusters. Only results for shells where the cooling time is less than 15 Gyr are shown. The center of the cluster is the leftmost data point for each cluster. Pressure and temperature are derived from the single temperature model fits.

ature T_h of the form (see Fig. 3):

$$r_c \sim T_h^{1.84 \pm 0.14}. \quad (2)$$

However, the virial radius scales proportional to $T_h^{0.5}$. This implies that r_c/r_{vir} is not constant from cluster to cluster.

Finally, the gas pressure is not constant in the core of our clusters. Our data confirm this well-known fact (see Fig. 4).

3. Multiphase Gas

3.1. Evidence for Multi-phase Gas

In the previous section we showed results for our single temperature fits. Although the single temperature fits are a good first-order approximation to the observed spectra, there are limitations to this model. Often the χ^2 values of our best fits are enhanced for the central

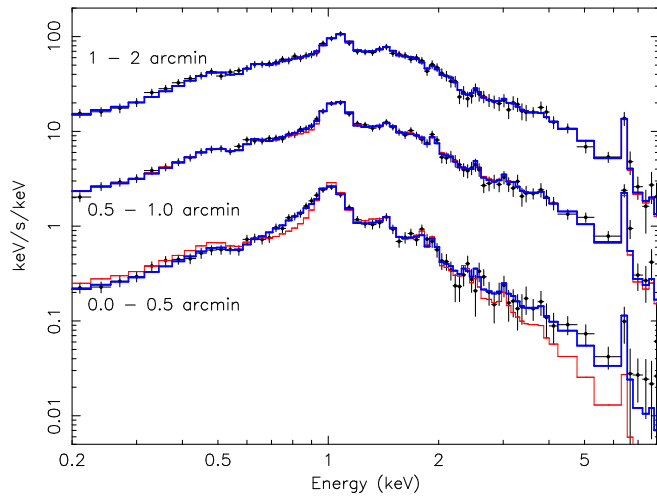


FIG. 5.— Spectrum of A 2052 in the inner three shells (with cooling gas). The spectra of all three EPIC camera’s have been added. The spectra of the 0.5–1.0’ and 1–2’ shells have been multiplied by factors of 5 and 25, respectively. The spectra are shown as energy times counts/s/keV. Thin solid histograms, red: fits with a single temperature model; thick solid histograms, blue: fits with the *wdem* model described in the text.

shells. Fig. 5 shows an example for this. In the central annulus, the spectrum shows an excess at high energies as compared to the single temperature model. Also, the Fe-L complex around 1 keV appears to be broader than predicted by the single temperature model. Instead, a good fit can be obtained by introducing more temperature components. In this case, the temperature of the dominant component becomes slightly larger in order to produce a slightly harder Bremsstrahlung continuum at higher energies (as well as the corresponding Fe-K line emission); in order to compensate for this temperature increase, cooler components are needed that better reproduce the low energy part of the Fe-L line blend.

3.2. How to Fit Multi-temperature Plasmas

In the previous section we have seen evidence for the presence of multi-temperature structure at the same radius. A powerful tool to investigate multi-temperature structure is to use the differential emission measure distribution (DEM). The DEM gives the emission measure (volume integral over electron density times hydrogen density) as a function of temperature T . We will use such a DEM approach in order to study the cooling gas in our clusters.

In order to make a proper model for the cooling gas, the following should be noted. The X-ray line spectra are insensitive to the details of the differential emission measure distribution (DEM) within a temperature range of a factor of two. This is illustrated in Fig. 6. All DEMs in that example have the same average temperature and an almost indistinguishable spectrum. For example, the black and red curve differ only in the width (Gaussian σ 0.02 and 0.10, respectively), but the average spectrum of a 0.90 keV and 1.10 keV plasma is almost the same as for a 1.0 keV plasma. In a similar way, there is in practice no way that the spectrum corresponding to the green,

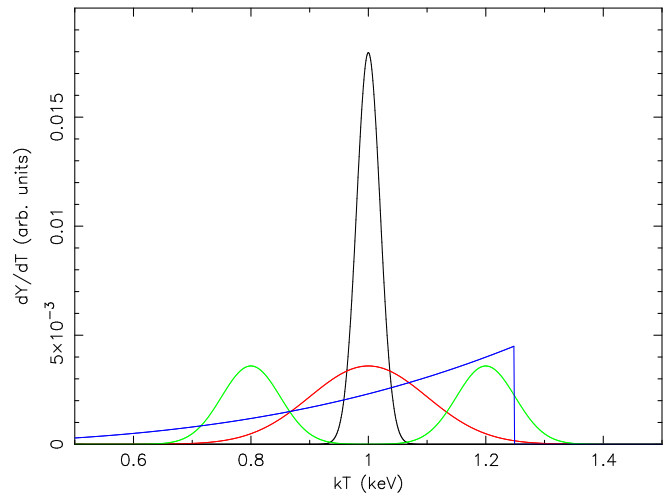


FIG. 6.— Four different differential emission measure distributions (DEM) all sharing the same emission-measure weighted average temperature and the same integrated emission measure. The corresponding X-ray spectra are almost indistinguishable.

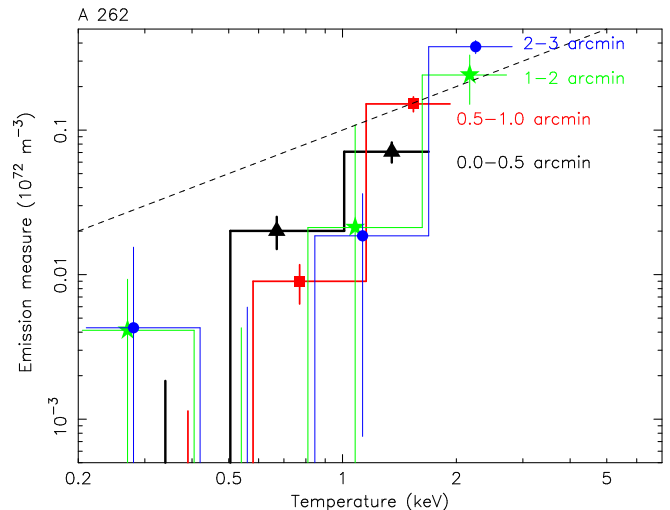


FIG. 7.— Emission measure distribution for the four innermost shells of A 262. Each color corresponds to a different annulus. The dashed line is the expected slope for an isobaric cooling flow model.

bimodal curve can be distinguished from the spectrum of the black or red curve. Even a skewed distribution like the blue curve yields a similar spectrum. We can conclude that if the DEM is decomposed as the sum of a few discrete temperature components, a binning by a factor of two in temperature is sufficient. All fine structure is effectively washed out, the only important thing is that the discrete components have the proper temperature centroid and emission measure integral over the relevant narrow temperature range.

We have applied such an approach to all our clusters. Each deprojected shell spectrum was fit with a multi-temperature model (we considered a maximum of 5 components). The temperature of the hottest component is a free parameter, the other temperature components are tied to this hot component by fixed multiplication factors of 0.5, 0.25, 0.125, and 0.0625. Also the emission

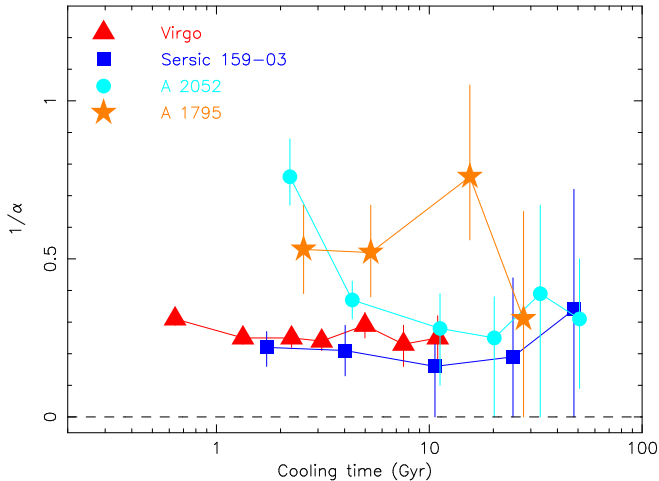


FIG. 8.— Steepness of the differential emission measure distribution (as represented by $1/\alpha$) versus cooling time for four clusters as indicated on the plot.

measure of all five components was a free parameter (as well as the abundances; however we tied the abundances of all components to the abundances of the hottest component). Fig. 7 shows an example of our results for the cluster A 262. This figure clearly shows a few characteristics that are found in all our clusters. First, the maximum temperature T_{\max} increases as function of radius r . Secondly, at each radius there is multi-phase plasma: we see evidence for at least two temperature components. Finally, the DEM at each radius is much steeper than expected from the standard isobaric cooling flow model.

3.3. Parameterization of the DEM

The multi-temperature fitting as employed in the previous section is a useful tool to investigate whether the gas is isothermal or multi-phase. However, multi-temperature fitting as done here sometimes gives large error bars on the DEM. This is due to the fact that if the spectrum shows weak emission above T_{\max} (either true or due to noise), the multi-temperature model may increase T_{\max} in order to accommodate for this high temperature tail by adjusting all values of the emission measures accordingly, yielding almost the same best-fit χ^2 , but with larger error bars on the derived emission measures.

Parameterized models are more stable but less general. However, we obtained excellent fits with the following parameterization:

$$\frac{dY}{dT} = \begin{cases} cT^\alpha & \text{if } T < T_{\max}; \\ 0 & \text{if } T \geq T_{\max}. \end{cases} \quad (3)$$

For $\alpha \rightarrow \infty$, the model becomes isothermal. We can summarize the results of our fits with the above spectral model as follows.

For most clusters, α is constant as a function of radius r (see Fig. 8 for an example; note that the cooling time is an increasing function of radius). For cooling times larger than 10–20 Gyr, the error bars on $1/\alpha$ are in general large, and include the value 0, which indicates that the spectra are consistent with an isothermal model in the

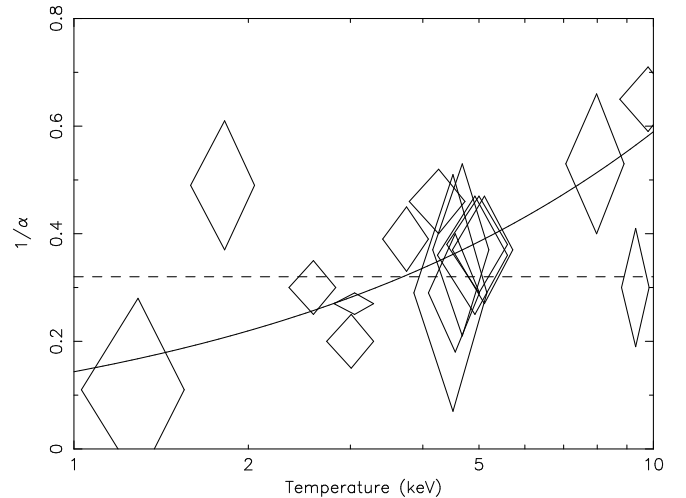


FIG. 9.— Steepness of the differential emission measure distribution versus maximum temperature. The diamonds represent the data points with error bars. The dashed line indicates the weighted average value of $1/\alpha$, the solid line the best fit power law scaling as described in the text.

outer parts of the cluster. The slightly enhanced values of $1/\alpha$ in a few rare cases at these locations are probably due to azimuthal temperature variations or other irregularities at larger distance from the core of the cluster. In the cooling region (cooling times less than 10–20 Gyr), none of our clusters shows a significant variation of α versus cooling time (and hence radius). Only in three cases (NGC 533, A 262 and A 2052) the innermost shell shows an enhanced value of $1/\alpha$ (see Fig. 8 for the case of A 2052). Perhaps in these cases an additional soft spectral component related to the central galaxy is present.

Furthermore, the average value of α for all the clusters in our sample is 3.1 ± 0.2 (see Fig. 9). Thus, at each radius in the cooling region the emission measure distribution decreases rapidly, proportional to $T^{3.1}$. There is a weak indication that $1/\alpha$ is slightly larger for the hotter clusters, see Fig. 9. Fitting formally a power law yields $\alpha = (7.1 \pm 1.2)T^{-0.61 \pm 0.13}$, where T is in keV. However, this fit is driven by only a few cool or hot clusters, so more data is needed to confirm such a correlation.

4. Discussion

4.1. Central Active Galactic Nucleus

Several explanations for the failure of the isobaric cooling flow model have been proposed. We do not summarize these here. Instead, we investigate whether our data can tell something about one of the most promising models, heating by a central Active Galactic Nucleus (AGN). To do that, we compare the radio luminosity at 1.4 GHz with the X-ray luminosity within the cooling radius. We find a clear correlation between both quantities. Interestingly, such a correlation was not found in a similar analysis based upon *Chandra* data (Voigt & Fabian 2003), however they used luminous cooling clusters (X-ray luminosity within the cooling radius $> 10^{37}$ W), while we also include less luminous cooling clusters. This correlation could be consistent with a heating by the central

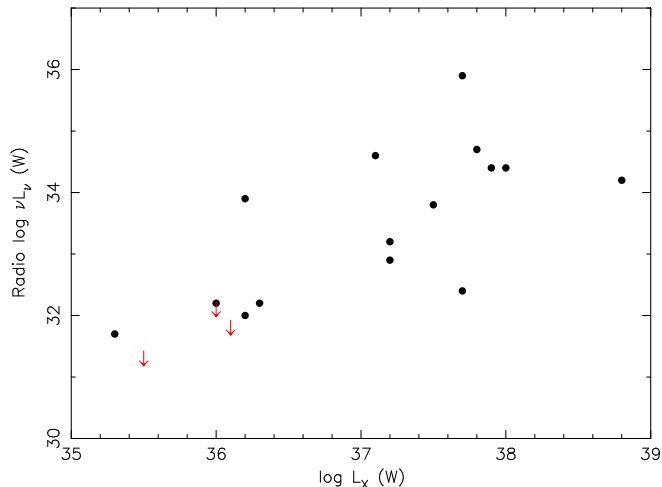


FIG. 10.— Correlation between the 0.2–10 keV X-ray luminosity within the cooling radius r_{cool} and $\nu L(\nu)$ at 1.4 GHz for the central radio galaxy. Upper limits are indicated by an arrow.

AGN scenario, but a correlation alone is insufficient proof for this. First, the correlation may be due to some selection effect or common “hidden” variable to which both L_X and L_{AGN} correlate. Furthermore, radio flux alone is not a proper measure of the time averaged power of an AGN. The relation between total power and observed radio luminosity is not perfect, due to intrinsic differences in radio loudness and orientation (beaming) effects, as well as the fact that radio and X-rays look at different time scales.

4.2. Magnetic Loops

The DEMs of the cooling cores of our clusters show a striking similarity to the DEMs of stellar or Solar coronal loops. In fact, the same physical processes are acting in both stellar coronae and clusters of galaxies: heat conduction along the magnetic field B and radiative cooling. We have modeled our DEMs in terms of the solar coronal loop models of Aschwanden & Schrijver (2002).

As an example we have worked out here the innermost three shells of 2A 0335+096. The cooling time in these shells is less than the age of the universe, and all three shells have significant multi-temperature structure. From the measured emission measure distribution we obtain the loop parameters. The loops have a typical length of 0.25–0.50 times the radius R where the loops are located. In the outermost shell this is in fair agreement with the magnetic field reversal length as obtained from numerical simulations of non-cooling regions (e.g., Dolag et al. 2002), in the innermost shell it is significantly smaller. However, the number of loops needed is large. The large number of loops as well as their small size then imply a highly tangled magnetic field structure in the central part of the cluster. A large number of loops also causes a relatively smooth surface brightness, consistent with detailed X-ray mapping of several clusters.

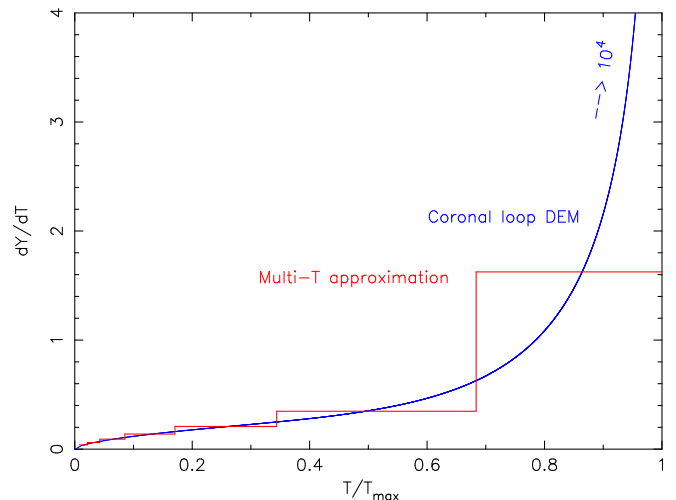


FIG. 11.— Differential emission measure for a solar coronal loop (blue curve) and multi-temperature approximation to it as used in our analysis (red histogram). For each temperature bin in the red histogram, the blue curve has the same integrated emission measure and average temperature as the red histogram. Note that for T close to T_{max} , near the top of the loop, the emission measure of the coronal loop becomes very large (due to the fact that $dT/dr = 0$ at the loop top).

5. Conclusions

The main results of our study can be summarized as follows.

1. The cooling region cannot be described by a single temperature at each radius. Instead, there is multi-temperature structure, however with a strong cut-off at low temperatures.
2. The DEMs are inconsistent with the standard isobaric cooling flow model.
3. The DEMs are steep, $dY/dT \sim T^3$ is a fair approximation for the DEM at each radius (with the maximum temperature T_{max} decreasing inwards).
4. Our results are in good agreement with the RGS results (Peterson et al. 2003).

This work is based on observations obtained with *XMM-Newton*, an ESA science mission with instruments and contributions directly funded by ESA Member States and the USA (NASA). The Space Research Organization of the Netherlands (SRON) is supported financially by NWO, the Netherlands Organization for Scientific Research. MSSL is supported financially by the UK Particle Physics and Astronomy Research Council.

References

- Allen S.W., Schmidt R.W., & Fabian A.C. 2001, MNRAS, 328, L37
Aschwanden, M.J., & Schrijver, C.J. 2002, ApJSupp, 142, 269
Blanton, E.L., Sarazin, C.L., & McNamara, B.R., 2003, ApJ, 585, 227
David, L.P., Nulsen, P.E.J., McNamara, B.R., Forman, W., Jones, C., Ponman, T., Robertson, B. & Wise, M. 2001, ApJ, 557, 546
Dolag, K., Bartelmann, M., & Lesch, H. 2002, A&A 387, 383
Kaastra, J.S., Ferrigno, C., Tamura, T., Paerels, F.B.S., Peterson, J.R. & Mittaz, J.P.D. 2001, A&A, 365, L99
Kaastra, J.S., Tamura, T., Peterson, J.R., Bleeker, J.A.M., Ferrigno, C., Kahn, S.M., Paerels, F.B.S., Piffaretti, R., Branduardi-Raymont, G., & Böhringer, H. 2003, A&A, in press (astro-ph/0309763)
Lewis, A.D., Stocke, J.T., & Buote, D.A. 2002, ApJ, 573, L13
Matsushita, K., Belsole, E., Finoguenov, A., & Böhringer, H. 2002, A&A, 386, 77
Molendi, S., & Pizzolato, F. 2001, ApJ, 560, 194
Peterson, J.R., Paerels, F.B.S., Kaastra, J.S., Arnaud, M., Reiprich, T.H., Fabian, A.C., Mushotzky, R.F., Jernigan, J.G. & Sakelliou, I. 2001, A&A, 365, L104
Peterson, J.R., Kahn, S.M., Paerels, F.B.S., Kaastra, J.S., Tamura, T., Bleeker, J.A.M., Ferrigno, C., & Jernigan, J.G. 2003, ApJ, 590, 207
Sakelliou, I., Peterson, J.R., Tamura, T., Paerels, F.B.S., Kaastra, J.S., Belsole, E., Böhringer, H., Branduardi-Raymont, G., Ferrigno, C., den Herder, J.W., Kennea, J., Mushotzky, R.F., Vestrand, W.T., & Worrall, D.M. 2002, A&A, 391, 903
Tamura, T., Kaastra, J.S., Peterson, J.R., Paerels, F.B.S., Mittaz, J.P.D., Trudolyubov, S.P., Stewart, G., Fabian, A.C., Mushotzky, R.F., Lumb, D.H., & Ikebe, Y. 2001a, A&A, 365, L87
Tamura, T., Bleeker, J.A.M., Kaastra, J.S., Ferrigno, C., & Molendi, S. 2001b, A&A, 379, 107
Voigt, L.M., & Fabian, A.C. 2003, MNRAS, submitted (astro-ph/0308352)